Increased depth of focus in random-phase-free holographic projection

Michal Makowski[1,*], Tomoyoshi Shimobaba[2], and Tomoyoshi Ito[2]

[1]*Warsaw University of Technology, Faculty of Physics, Warsaw 00-662, Poland*
[2]*Graduate School of Engineering, Chiba University, 1-33 Yayoi-cho, Inage-ku, Chiba 263-8522, Japan*
**Corresponding author: michal.makowski@if.pw.edu.pl*

Received September 13, 2016; accepted October 28, 2016; posted online November 29, 2016

The recently proposed random-phase-free method enables holographic reconstructions with very low noise, which allows fine projections without time integration of sub-holograms. Here, we describe the additional advantage of this method, namely, the extended depth of sharp imaging. It can be attributed to a lower effective aperture of the hologram section forming a given image point at the projection screen. We experimentally compare the depth of focus and imaging resolution for various defocusing parameters in the cases of the random-phase method and the random-phase-free method. Moreover, we discuss the influence of the effective aperture in the presence of local obstacles in the hologram's plane.

OCIS codes: 090.1705, 090.1760, 090.2870, 090.5694.
doi: 10.3788/COL201614.120901.

The recent progress in phase-only spatial light modulator (SLM) has allowed lensless holographic projection of color images with unprecedented throwing angles of over 10°[1]. The pixel count of over 8M pixels and reduction of pixel pitch to 3.74 μm with the sustained fill factor of ~90% brings us closer and closer to practical applications of SLMs in the display industry. Nevertheless, because of the phase-only nature of light modulation, one needs to use iterative algorithms of phase optimization in order to shift the signal information from the amplitude part of the hologram to its phase part. The consequence of using, e.g., the Gerchberg–Saxton (GS) algorithm[2] is the random-like pattern of the iterated phase distributions. This, in turn, leads to random phase relations in the resulting images reconstructed from such diffuse-type computer-generated holograms (CGHs) at the projection screen. The result is highly visible holographic noise. Numerous methods have been proposed to date, including fast display of sub-holograms with different initial phases (the time-domain random-phase method[3]) and the spatial interleaving of the displayed image points (the pixel separation method[4]). Inconveniently, all the said methods require a fast refresh rate of the SLM in order to provide satisfactory results of noise suppression to the industry-accepted noise level of 2%. The term "noise level" used in this work is defined as the standard deviation of the light intensity in the test uniform region divided by the average intensity.

The major breakthrough in noise management in holographic projection was the introduction of the random-phase-free (RPF) method by Shimobaba and Ito[5,6], further improved by iterative optimization[7]. The method assumes the ordered initial phase distribution of a convergent kinoform lens.

Figure 1 shows the geometric setup of the CGH calculation using the RPF method. An object $u_i(x_i, y_i)$ is multiplied with the virtual convergent kinoform lens $w(x_i, y_i) = \exp(i\pi(x_i^2 + y_i^2)/\lambda f_i)$, where λ is the wavelength and f_i is the focal length of the convergent lens. Then, to obtain the complex amplitude in the CGH plane, we calculate the numerical diffraction from the object plane to the CGH plane. The value of f_i is set to the distance at which the CGH just fits into the cone of the convergence light. Therefore, f_i is determined by the following simple relation, $S_h : S_i = z_1 : f_i$, where S_h and S_i are the areas of the CGH and object, and z_1 is the distance between the CGH and the focal point.

The RPF method allows the smooth and slowly varying final phase of Fresnel-type CGHs. Figure 2 compares the magnified parts of two holograms of the same input image calculated with the GS and RPF methods. Obviously, the smooth nature of the phase obtained using the RPF method results in ordered phase relations of the light rays forming the intensity image on a projection screen. Figure 3 shows the experimental projections of the test

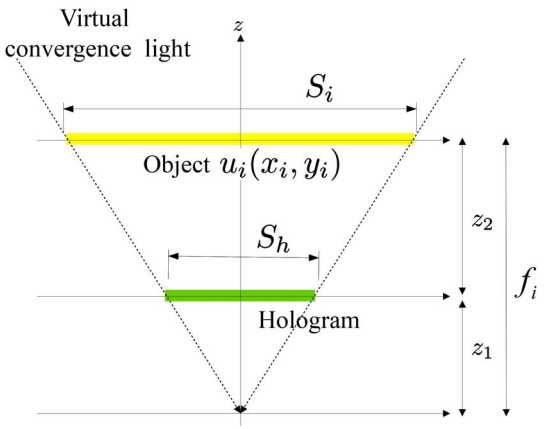

Fig. 1. Geometric setup of the CGH calculation using the RPF method.

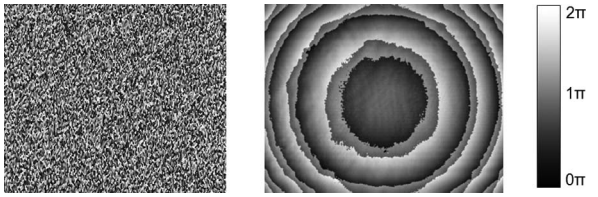

Fig. 2. Magnified parts of CGHs computed with GS algorithm (left) and RPF method (right).

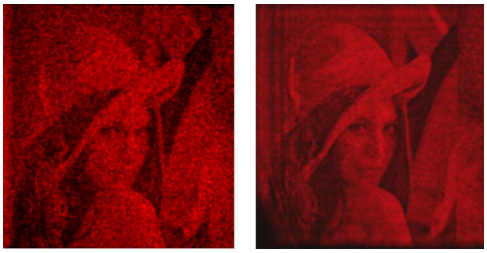

Fig. 3. Experimental projections of a test image on a projection screen with the GS method (left) and the RPF method (right).

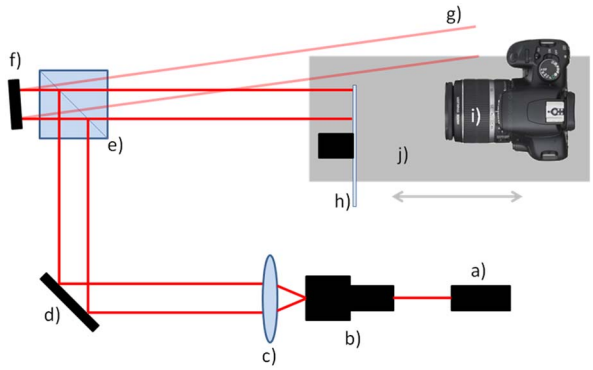

Fig. 4. Optical setup for the measurement of the depth of focus in a holographic projection: (a) He–Ne laser, (b) pinhole, (c) lens, (d) mirror, (e) 50–50 non-polarizing beam splitter, (f) SLM, (g) zero-order light, (h) screen (a revolving diffuser), (i) digital camera, and (j) moving carrier stage.

input image at a distance of 1000 mm. The GS image has a noise level of 17%, while the RPF image has a noise level of only 5%.

The images were obtained with a Canon 650D digital camera from the Holoeye Pluto SLM with an 8 μm pixel pitch illuminated with a quasi-plane wave from an He–Ne laser at 632.8 nm, as shown in Fig. 4. The image size at the screen was ~30 mm × 30 mm. The diffuser was used as the screen in order to observe in-line, not geometrically distorted images. The diffuser was revolving at ~300 RPM so as to time average the laser speckles originating from its diffusive surface. In order to achieve this, long-enough exposures of ~200 ms were used.

The distance from the screen to the camera was fixed, and the camera was focused carefully on a rotating diffuser. The camera and screen were mounted on a common carrier stage, which was then moved freely along the direction of projection by the SLM, with 1000 mm as the base distance. By the proper measurement of the distance between the SLM and the diffuser, the defocus was calculated, and thus the experimental assessment of the depth of focus (DoF) was done. The photographs were taken in RAW format with a resolution of 5184 × 3456 pixels.

The shallow depth of focus in holographic projections is a major problem, because in improvised projections, the focusing distance has to be adjusted in real time. In order to do that, the focusing power of the lens factor encoded in CGHs must be constantly recalculated, which involves significant computational power, especially in handheld, battery-operated devices. As known from the fundamentals of imaging, the depth of focus depends on the angular variance of the light rays forming the image[8]. In pinhole imaging, all the rays propagate at almost the same angle, leading to a DoF. On the other hand, when diffusive-type CGHs calculated with the GS method are used for image formation, the angles of the rays are highly variable, causing a limited depth of focus, estimated to ~10 mm for a projection distance of 1000 mm. Figure 5 schematically shows the difference in DoF for the GS and RPF methods. Note that the extended DoF is highly suitable for the holographic 2D projection shown in this work, but on the other hand, it makes displaying 3D objects impractical, as the spatial points of such objects would be far less localized along the optical axis.

The optically obtained images of the same size for variable defocus distances are gathered in Figs. 6 and 7. One can easily notice that the readability of the test USAF pattern in RPF is sustained even for strong defocusing of 90 mm, while the GS holograms form sharp images only for the defocusing below 30 mm. Note that GS images were obtained by a time integration of 10 sub-holograms in order to suppress the holographic noise to a level low

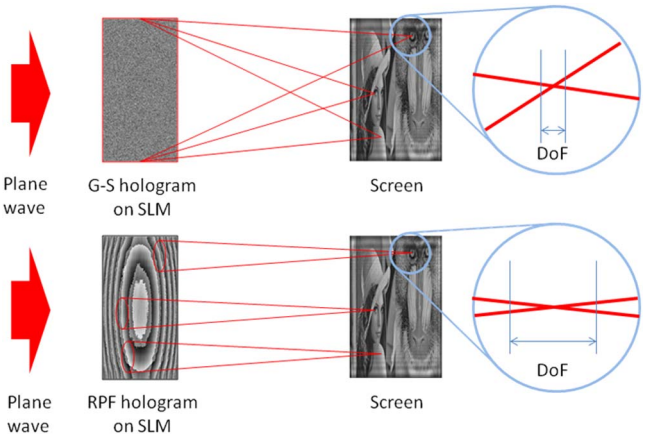

Fig. 5. Shallow depth of focus in diffuse-type computer hologram computed with GS method (top) and increased depth of focus in an RPF hologram (bottom). The circles on the SLM mark the size of the effective aperture.

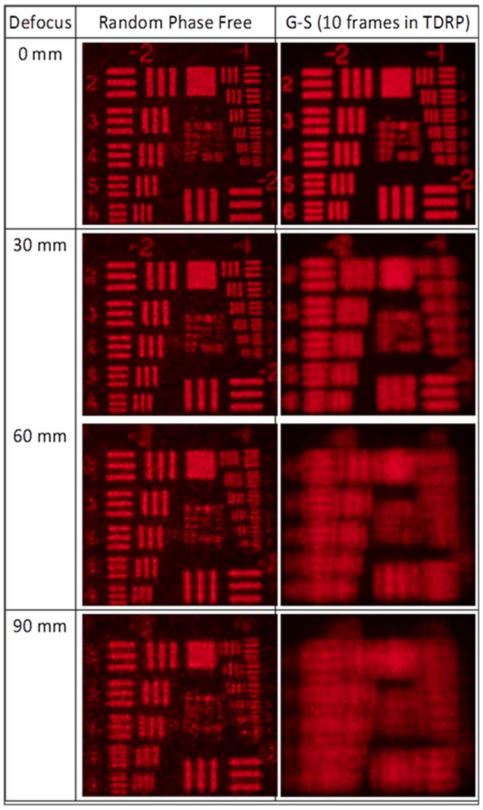

Fig. 6. Experimental comparison of the defocused holographic images obtained with GS and RPF methods (USAF 1951 test pattern).

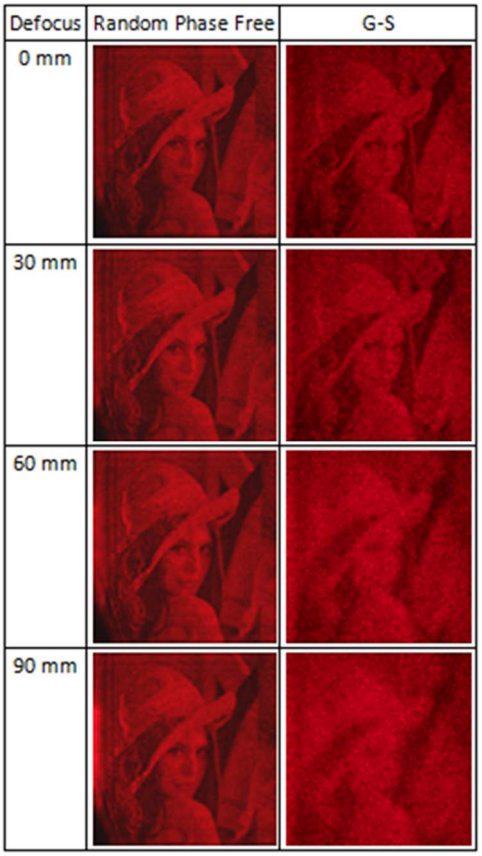

Fig. 7. Experimental comparison of the depth of focus in the GS and RPF methods (Lena).

enough to allow the assessment of the image resolution, while the RPF images were obtained from a single hologram. This underlines the significantly smaller computational requirements of the RPF method in real-time holographic projections.

In order to quantify the effect of the increase of the DoF on the RPF method, two methods were used. In the first attempt, the smallest resolved section of the USAF pattern was selected by a human observer as a function of the defocusing. The results averaged for the horizontal and vertical cases are shown in Fig. 8. The RPF method is superior in terms of image resolution when the defocusing exceeds 15 mm.

In the second attempt, an edge response test was performed, i.e., the widths of the edges of the white square elements of a USAF pattern on a black background were measured. The widths were between 10% and 90% of the maximal value of brightness. The results for the vertical and horizontal cases, measured in camera pixels, were averaged and plotted against the defocus distance (see Fig. 9).

The RPF method is superior in the entire region of used defocus values. The error seen in the experimental series mainly comes from the holographic noise present in the examined area of the edges (see Fig. 10).

The area of the used SLM was constant, but the change of the CGH algorithm increased the depth of focus. This effect must be due to a limited aperture of imaging when the RPF method is used, further referred to as the effective aperture. We expect that this effect should exist for any given projection distance; nevertheless, in this study, we present experimental results for a single base distance of 1000 mm. As shown in Fig. 5, each point in the image is formed by the limited circular effective aperture, as opposed to the GS method, where the effective aperture is equal to the physical aperture of the SLM. In order

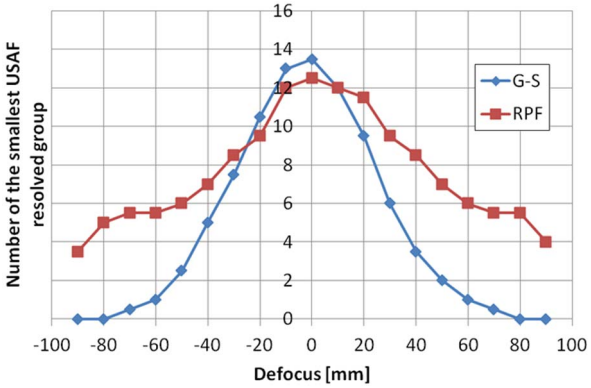

Fig. 8. Smallest resolved group of the USAF test pattern as a function of defocusing at a base distance of 1000 mm for the GS and RPF methods.

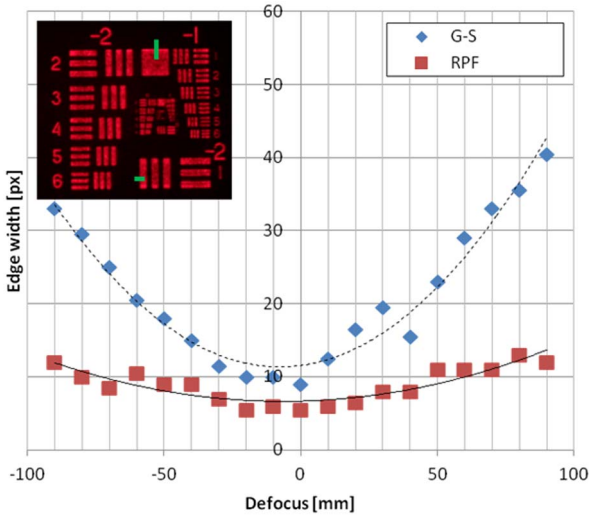

Fig. 9. Experimental 10%–90% edge response as a function of defocusing at a base distance of 1000 mm for the GS and RPF methods. Dashed and solid lines are fittings with quadratic functions. The inset shows the vertical and horizontal edges taken for the test (green).

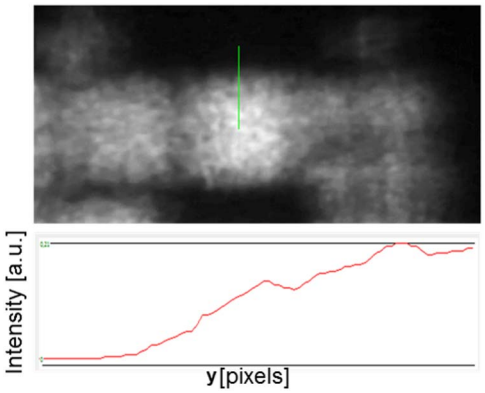

Fig. 10. Problematic assessment of the edge response in the presence of holographic noise (upper). Exemplary cross-section is shown along the green line (bottom).

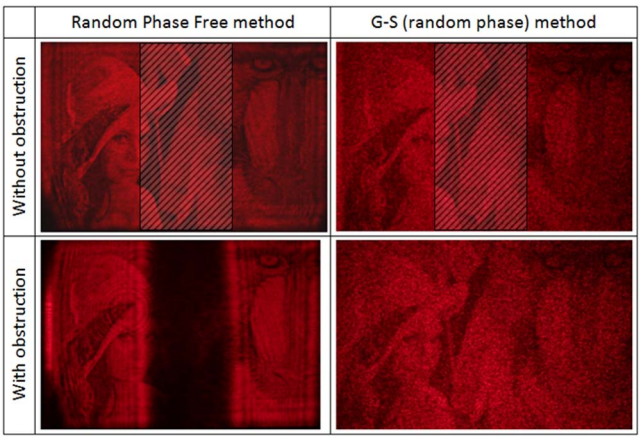

Fig. 11. Introduction of an obstruction (marked in the upper row) to the SLM plane causes a shadow in the RPF case.

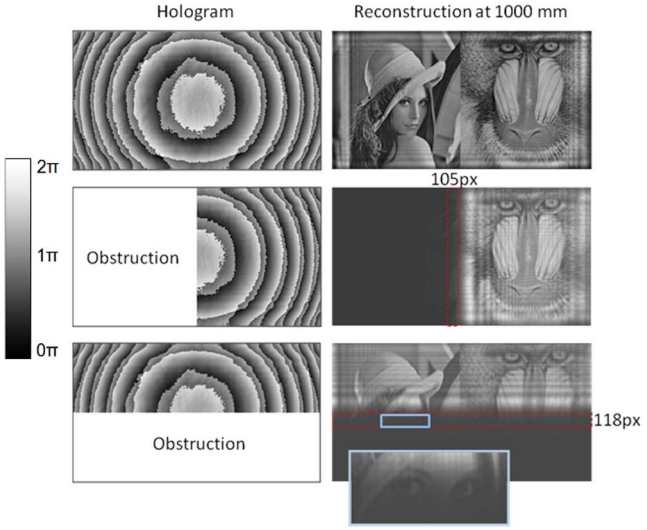

Fig. 12. Numerical simulation of the shadow caused by the obstruction of half of the SLM area. A magnified zone of the intensity decay is shown in the blue frame.

to evaluate the size of the effective aperture, an obstruction was introduced in the SLM plane in order to examine the resultant distribution of a shadow on the screen (see Fig. 11).

The size of the area where the intensity drops from the maximal value to zero carries the information about the size of the effective aperture. Nevertheless, its assessment was difficult because of the noise and weak light intensity; therefore, the numerical simulations of obstructing half of the SLM were performed as shown in Fig. 12. The calculation matrix was 2048×2048 points with sampling equal to that of the used SLM (8 μm), $\lambda = 633$ nm.

The area of the intensity decay zone (marked with the red dashed line in Fig. 12) was measured to be ~111 pixels (888 μm) wide (i.e., the average of values 105 and 118 px). Therefore, one can draw the conclusion that each infinitesimally small fraction of the SLM area forms the circular section of the image with a diameter of ~0.8 mm. Simultaneously, one can reverse this approach and claim that each point of the image is generated by a circular effective aperture on the SLM with the same diameter, i.e., 0.8 mm. Therefore, the presence of local obstructions of larger sizes

Fig. 13. Simulated loss of image points from an obstruction in the SLM plane.

at the SLM could lead to the loss of information in the projected image. Figure 13 shows the simulated loss of the image contents when the SLM is obstructed with a vertical bar 0.8 mm in width. This result additionally confirms the claim regarding the size of the effective aperture.

In conclusion, we use two alternative experimental methods to confirm that the RPF method of calculating holograms for projection offers greatly extended depth of sharp imaging, compared to classic methods based on a random initial phase. This important advantage originates from the fact that the hologram is no longer of the diffuse type; therefore, each section of the projected image has a direct connection with a dedicated area on the SLM. Unfortunately, this also disables the ability to suppress local defects and obstructions at the SLM, as is demonstrated here in the case of the GS type holograms. The balance between the increased tolerance of screen projection and diminished tolerance to local defects should be carefully chosen for a particular application. For example, in portable holographic projection, local defects of the SLM are far more likely than in stand-alone projectors with self-cleaning capabilities. Hence, the proposed RPF method is therefore suitable for the latter case, but in all cases, the real benefits of lower noise level and lower computational requirements are conveniently achievable.

This work was funded by the Polish National Centre for Research and Development (No. LIDER/013/469/L-4/12/NCBR/2013) and the Polish National Science Centre (No. 2015/17/B/ST7/03754).

References

1. M. Makowski, I. Ducin, K. Kakarenko, J. Suszek, and A. Kowalczyk, Photon. Lett. Poland **8**, 26 (2016).
2. R. W. Gerchberg and W. O. Saxton, Optik **35**, 237 (1972).
3. A. Czerwiński, K. Kakarenko, M. Sypek, M. Makowski, I. Ducin, J. Suszek, A. Kolodziejczyk, and J. Bomba, Opt. Lett. **37**, 4723 (2012).
4. M. Makowski, Opt. Express **21**, 29205 (2013).
5. T. Shimobaba and T. Ito, Opt. Express **23**, 9549 (2015).
6. T. Shimobaba, T. Kakue, Y. Endo, R. Hirayama, D. Hiyama, S. Hasegawa, Y. Nagahama, M. Sano, M. Oikawa, T. Sugie, and T. Ito, Opt. Express **23**, 17269 (2015).
7. T. Shimobaba, T. Kakue, Y. Endo, R. Hirayama, D. Hiyama, S. Hasegawa, Y. Nagahama, M. Sano, M. Oikawa, T. Sugie, and T. Ito, Opt. Commun. **355**, 596 (2015).
8. J. W. Goodman, *Introduction to Fourier Optics* (Roberts and Company Publishers, 2005).